

Original article

QSAR analysis of 1,4-dihydro-4-oxo-1-(2-thiazolyl)-1,8-naphthyridines with anticancer activity

Mariyana Atanasova, Sonia Ilieva*, Boris Galabov*

Department of Chemistry, University of Sofia, Sofia 1164, Bulgaria

Received 5 December 2006; received in revised form 22 January 2007; accepted 25 January 2007

Available online 25 February 2007

Abstract

In the present study a quantitative structure activity relationship (QSAR) analysis was applied to a series of 100 of 7- and 3-substituted 1,4-dihydro-4-oxo-1-(2-thiazolyl)-1,8-naphthyridine derivatives. The Chem-X (version 2000) software was used to develop 3D QSAR models. The steric and electrostatic interactions between a probe atom (H^+) and a set of aligned molecules were assessed using the comparative molecular field analysis method. Statistically relevant models were derived for both electrostatic and steric fields. A 2D model over a restricted series of close structural analogs was derived as well. A number of conclusions on the relationship between the type and size of different substituents and the antitumor activity of the compounds were derived.

© 2007 Elsevier Masson SAS. All rights reserved.

1. Introduction

A series of 7- and 3-substituted 1,4-dihydro-4-oxo-1-(2-thiazolyl)-1,8-naphthyridines as novel antitumor quinolone agents were synthesized and studied by Tomita and coworkers [1–3]. Among the compounds, SNS-595 is a potential anticancer agent and is in clinical trials. The purpose of our study is to gain insight into the structural features related to the anticancer activity of the compounds from the naphthyridine series by applying the QSAR methodology.

A number of quinolone derivatives are known for their antibacterial properties [4]. These compounds inhibit the bacterial DNA topoisomerase II enzymes gyrase and topoisomerase IV, which participate in the division of bacterial cells [5]. The mammalian enzyme topoisomerase II (topo II) has the ability to change the DNA topology by breaking the double helix DNA and allowing a chain transition [6]. It is well established that blocking of this enzyme terminates the further process of DNA replication [7]. This mechanism was the basis for the development of new antitumor agents, which are able to block the topoisomerase II enzyme. A number of drugs

were developed following this strategy. The agents that have found clinical application include etoposide, doxorubicin, ellipticine and amsacrine [8]. The mechanism of action of the mammalian topo II enzyme is similar to that of bacterial DNA gyrase/topoisomerase IV. Many antibacterial quinolones were assessed regarding their ability to induce mammalian topoisomerase II-mediated DNA cleavage in vitro and were found to form a promising new class of antitumor agents [9–17]. Different types of quinolones have been reported to possess the activity as inhibitors of topoisomerase II. No derivative from this group has, however, reached clinical trials. The topoisomerase II-mediated DNA cleavage in eukaryotic cells is also the target of 6,8-difluoroquinolone derivatives [18–20]. In vivo studies of the mechanism of action of the most active compound from this series, 6,8-difluoro-7-(4-hydroxyphenyl)-1-cyclopropyl-4-quinolone-3-carboxylic acid (CP-115,953) was examined by Elsea et al. [21]. The authors concluded that the principal target of the quinolones as cytotoxic agents is the topo II enzyme. These authors also discussed that compound CP-115,953 exerts its cell killing activity via the topo II enzyme turning it into a cell poison. The derivative 1-cyclopropyl-6,8-difluoro-1,4-dihydro-7-(2,6-dimethyl-4-pyridinyl)-4-oxo-3-quinolinecarboxylic acid (WIN57294) inhibits the mammalian topo II [22]. Similar

* Corresponding authors.

E-mail address: galabov@chem.uni-sofia.bg (B. Galabov).

activity leading to DNA untwining exhibits also two quinobenzoxazines derivatives [23,24]. Several 1,8-naphthyridines were reported to possess antitumor activity [25–35]. Their activity is linked to inhibition of the tubulin polymerization. Derivatives of quinolin-4-one and 1,7-naphthyridin-4-one were also reported as potential anticancer agents due to inhibition of cdc25 phosphatase [36]. In spite of the extended studies on quinolone based antitumor agents, so far no derivative from this group has gone to clinical tests.

In the search of novel antitumor quinolone agents targeting the topo II enzyme, Tomita and coworkers [1–3] synthesized and studied for anticancer activity substituted at different positions of 1,8-naphthyridine derivatives. The authors found that the compounds possess from moderate to pronounced cytotoxic activity against several murine and human cell lines. Among the series of 7-(3-aminopyrrolidinyl) derivatives, the compound 7-((3*S*,4*S*)-3-methoxy-4-(methylamino)pyrrolidin-1-yl)-4-oxo-1-(thiazol-2-yl)-1,4-dihydro-1,8-naphthyridine-3-carboxylic acid (AG-7352, SNS-595 or SPC-595) possesses potent cytotoxicity in both in vitro and in vivo assays [2] (Fig. 1). The derivative shows a more potent anticancer activity against human tumor cell lines than etoposide [2]. At present SNS-595 is in clinical trials, phases I and II. The compound showed an excellent antitumor activity against a considerable number of tumor cell lines [37]. SNS-595 possesses also antitumor activity in the cases of human xenograft tumor models as well as murine syngeneic models, including cases of drug resistant models [37]. It was found that SNS-595 causes a regression of the highly metastatic syngeneic Colo-26 tumor model, known to its resistance to the main classes of cytotoxic agents [37]. It was also found that SNS-595 could be effectively combined with a wide variety of cytotoxic drugs, chemotherapeutic modulators and novel agents that are active in S-phase or regulate non-homologous end-joining (NHEJ) repair or apoptosis signalling [38].

The mechanism of action of SNS-595 was studied in detail [39–43]. It was established that SNS-595 is a novel cell cycle modulator acting during the S-phase (the phase of DNA synthesis). It causes a significant S-phase lag and irreversible

G2 arrest (the gap in time between mitosis and the next cycle of DNA synthesis) with 4N DNA content. This cell cycle arrest is rapidly followed by the onset of apoptosis, which is mediated through p53 independent and dependent mechanisms [37,40,41]. SNS-595 differs from the typical G2 studied therapeutic arrestors and S-active compounds in causing significant S-phase lag as well as definite G2 arrest [40]. It was found that topoisomerase II is not the target of SNS-595 [40]. Recent investigations showed that SNS-595 is a double strand break agent [43]. The metabolism of SNS-595 was investigated in vitro and in vivo [38]. It was found that it metabolises minimally and does not inhibit or induce the CYP450 enzyme system [38]. These findings characterise SNS-595 as a promising anticancer agent.

In the present study a series of 100 compounds of 7- and 3-substituted 1,4-dihydro-4-oxo-1-(2-thiazolyl)-1,8-naphthyridines were subjected to QSAR analyses. The goal of our research was (i) to gain further insight into the structural features related to the anticancer activity of the compounds from the quinolone series and (ii) to suggest new substituents or structures with potentially enhanced anticancer activity.

2. Methods

2.1. Compounds studied and biological activity data

The compounds investigated in the present study represent a series of 100 7- and 3-substituted 1,4-dihydro-4-oxo-1-(2-thiazolyl)-1,8-naphthyridines. As mentioned these compounds were synthesized and tested by Tomita and coworkers [1–3]. One compound from the series – 7-((3*S*,4*S*)-3-methoxy-4-(methylamino)pyrrolidin-1-yl)-4-oxo-1-(thiazol-2-yl)-1,4-dihydro-1,8-naphthyridine-3-carboxylic acid (SNS-595, AG-7352, or SPC-595) possesses more potent cytotoxicity against human tumor cell lines than the known anticancer drug etoposide [2]. At present SNS-595 is considered a promising anticancer agent and it is in clinical trials, phases I and II.

The structural formulas of the compounds studied are shown in Fig. 2. We used literature data for their in vitro cytotoxic activity – IC_{50} , the concentration of the agent to reduce cell viability by 50%, against Murine P388 Leukemia [1–3]. The values of $\log(1/IC_{50})$, given in Table 1, are used in the present work.

2.2. Computational methods

The 3D QSAR analysis was performed using the molecular field analysis method as implemented in the Chem-X software [44] combined with weighted least squares method (WLS) for regional mapping, visualizing the results obtained.

The Fujita–Ban [45] modification of the Free–Wilson approach [46] was applied for 49 structures from the series studied in order to find a 2D QSAR model.

The simultaneous application to the same series of compounds, both 2D and 3D QSAR approaches are expected to provide internally consistent results [47]. The 2D QSAR methods are usually faster, more automated (since they

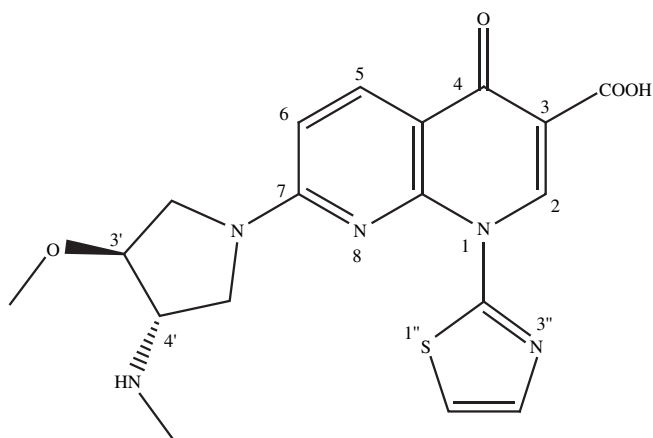


Fig. 1. Structure of SNS-595.

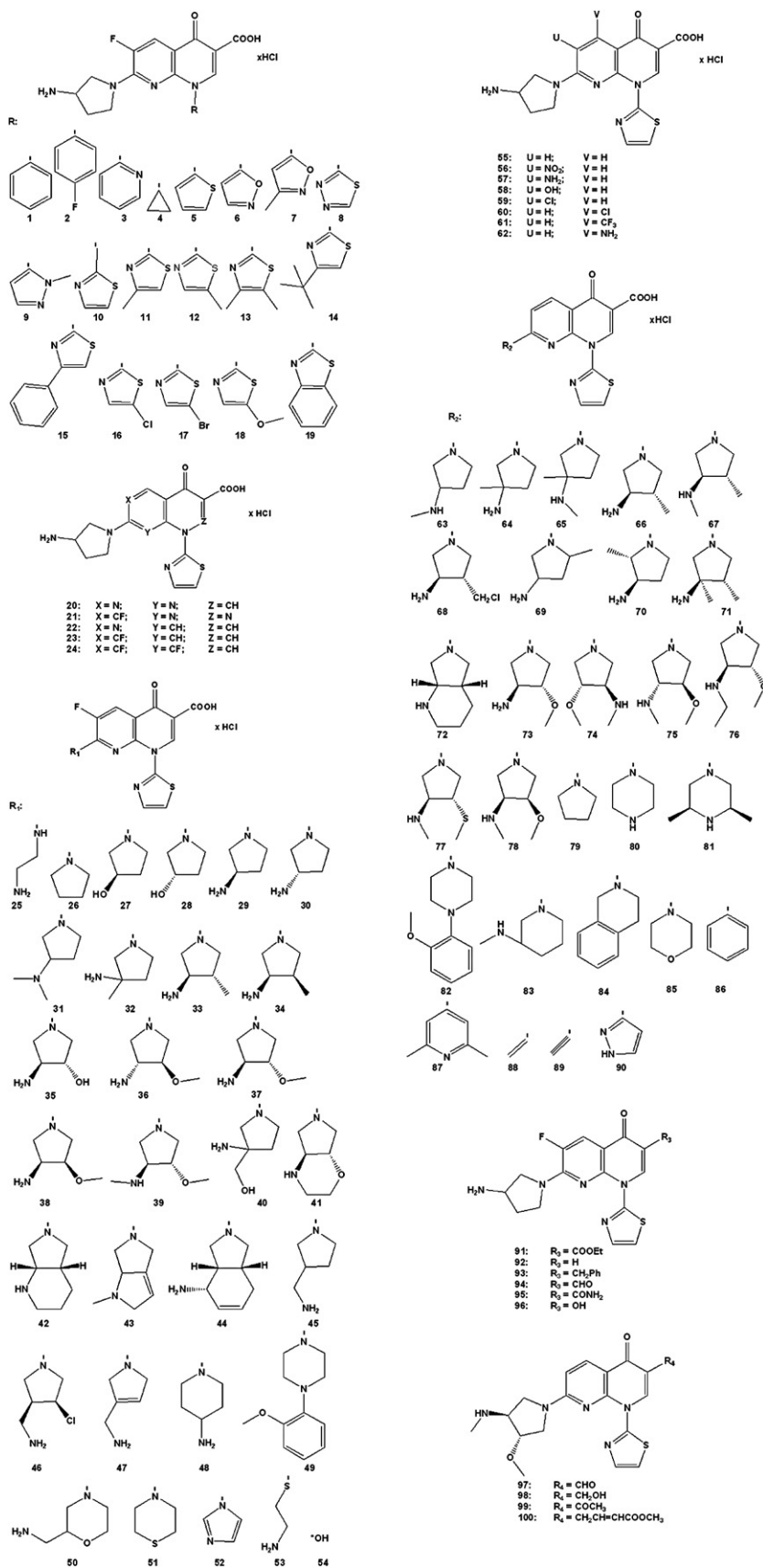


Fig. 2. Structures of 7- and 3-substituted 1,4-dihydro-4-oxo-1-(2-thiazolyl)-1,8-naphthyridines.

Table 1
Measured and transformed IC_{50} values for the series studied

No.	IC_{50} mol/L	$\log(1/IC_{50})$									
1	6.5153	-0.8139	26	0.0957	1.0191	51	4.4339	-0.6468	76	0.0602	1.2204
2	5.4355	-0.7352	27	0.1727	0.7627	52	27.9862	-1.4469	77	0.0479	1.3197
3	27.0746	-1.4326	28	0.0531	1.2749	53	27.2933	-1.4361	78	0.0498	1.3028
4	23.7716	-1.3761	29	0.0426	1.3706	54	32.5460	-1.5125	79	0.1928	0.7149
5	3.2052	-0.5059	30	0.0746	1.1273	55	0.0280	1.5528	80	0.1595	0.7972
6	26.1611	-1.4177	31	0.1413	0.8499	56	5.6911	-0.7552	81	0.2101	0.6776
7	1.5536	-0.1913	32	0.0668	1.1752	57	2.7121	-0.4333	82	2.1575	-0.3340
8	14.6135	-1.1648	33	0.0282	1.5498	58	11.5430	-1.0623	83	1.3491	-0.1300
9	26.8562	-1.4290	34	0.1464	0.8345	59	0.5793	0.2371	84	24.7254	-1.3931
10	25.6803	-1.4096	35	5.3401	-0.7275	60	0.1251	0.9027	85	0.3348	0.4752
11	0.1310	0.8827	36	0.1677	0.7754	61	0.2304	0.6375	86	18.1187	-1.2581
12	0.6677	0.1754	37	0.0567	1.2464	62	0.0218	1.6615	87	19.3733	-1.2872
13	0.4462	0.3505	38	0.2072	0.6836	63	0.0269	1.5703	88	3.3411	-0.5239
14	2.0395	-0.3095	39	0.0429	1.3675	64	0.0512	1.2907	89	7.7366	-0.8886
15	0.1152	0.9386	40	0.2072	0.6836	65	0.0467	1.3307	90	12.7900	-1.1069
16	0.2294	0.6394	41	2.3957	-0.3794	66	0.0258	1.5884	91	0.3371	0.4722
17	0.1871	0.7279	42	0.7318	0.1356	67	0.0311	1.5073	92	0.5281	0.2773
18	0.8633	0.0638	43	0.0919	1.0367	68	0.0591	1.2284	93	0.1703	0.7688
19	0.1152	0.9386	44	0.3509	0.4548	69	0.2962	0.5284	94	0.0590	1.2292
20	0.1311	0.8824	45	0.2594	0.5860	70	0.2531	0.5967	95	0.7185	0.1436
21	26.5699	-1.4244	46	0.3681	0.4340	71	0.0519	1.2848	96	0.4836	0.3155
22	2.7981	-0.4469	47	0.2168	0.6639	72	0.0428	1.3686	97	0.0802	1.0958
23	26.7102	-1.4267	48	4.1859	-0.6218	73	0.0465	1.3326	98	0.1422	0.8471
24	140.1703	-2.1467	49	2.0768	-0.3174	74	0.0187	1.7282	99	0.1484	0.8286
25	28.6254	-1.4568	50	4.2674	-0.6302	75	0.0523	1.2815	100	0.2079	0.6822

inherently lack the alignment problem), and the obtained cross-validated R^2 values are similar or exceed those in 3D analysis [48].

3. Results and discussion

3.1. 3D QSAR results

Each structure was drawn and converted into its three-dimensional counterpart using the Chem-X software [44]. Pre-optimisation of the molecular geometry was performed using the AMBER molecular mechanics force field as implemented in the Chem-X package [49]. The conformational space of each compound was searched using the systematic search method. Automatically selected single bonds from the program were rotated to 180 degrees using a 30 degree step. In the case of double bonds both cis- and trans-conformers were considered. All generated structures with improper van der Waals contacts were excluded from the calculations. The energy was computed using molecular mechanics with the AMBER force field. Conformers with lowest energy were then optimised by the MOPAC program applying AM1 semi-empirical quantum mechanical method.

An important step for a correct 3D QSAR analysis is the selection of a proper structure for superimposing the molecules. According to the key-lock principle in 3D QSAR [50], the most active compound in the series should have the geometry nearest to optimal for the ligand-receptor interactions. For this reason we chose compound **74** (7-((3*S*,4*S*)-3-methoxy-4-(methylamino)pyrrolidin-1-yl)-4-oxo-1-(thiazol-2-yl)-1,4-dihydro-1,

8-naphthyridine-3-carboxylic acid, SNS-595) as the template for aligning all the remaining molecules. Flexible fitting procedure was employed for superimposing all molecules from the series. Our field comparisons with flexible fitted structures are based on calculated RMS (root mean squares) errors, where the entire conformational space was explored in searching molecules with minimum RMS between them and molecule **74**. Only a single conformer for each molecule was used: the one that best fits the template. The result from the alignment procedure is shown in Fig. 3.

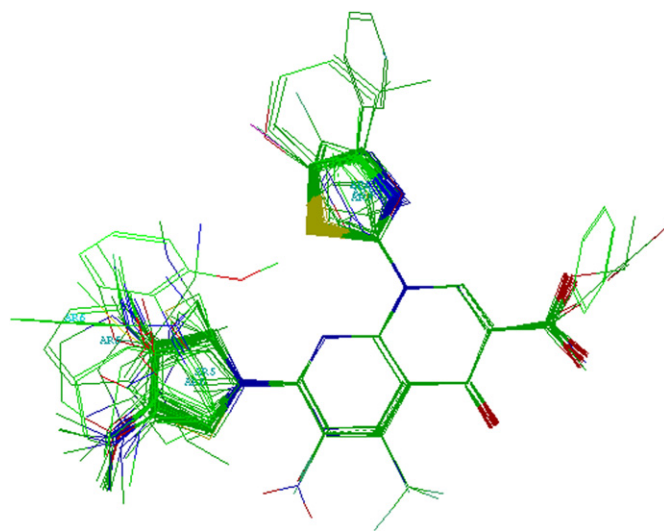


Fig. 3. Aligned structures for the series of 1,4-dihydro-4-oxo-1-(2-thiazolyl)-1,8-naphthyridines.

The next step was to build a 3D grid around the set of superimposed molecules using a grid constant of 1 Å. The probe atom is H⁺. The grid space is 4 Å bigger than the size of the largest molecules. The steric and electrostatic interaction energies between the probe atom and the set of aligned molecules were calculated for each gridpoint using 0.95 cut-off default for both fields.

The two-pass-PLS (partial least squares) method was used to obtain the 3D QSAR model. The first step in this method is to calculate the principal components and then to obtain the model and its statistical parameters. Eleven principal components (PCs) for both the steric and electrostatic interaction energies were generated. The program from the data table constructs a separate covariance matrix. The full eigen system of this matrix is determined by PLS using the singular value decomposition (SVD) method. The matrix is then rewritten in a new form, and the coefficients of the transformed variables (the principal component loadings) are evaluated and used to determine the principal component scores, a set of new variables which best explain the variance of the data.

For the steric and electrostatic fields the calculated PCs cover over 80% of the data dispersion. The following parameters were used as criteria for the internal predictive power of the model: the correlation coefficient, R^2 , the cross-validated correlation coefficient, Q^2 , and the internal predictive correlation coefficient, R_{pred}^2 . Q^2 was computed employing the leave-group-out procedure using randomly generated fifth subgroups of the train series. R_{pred}^2 was computed for 20% randomly selected molecules of the train set by the following equation:

$$R_{\text{pred}}^2 = 1 - \frac{\text{PRESS}}{\text{SSQ}} \quad (1)$$

$$\text{PRESS} = \sum_{p=1}^P (\text{obs}_p - \text{pred}_p)^2 \text{ and } \text{SSQ} = \sum_{p=1}^P (\text{obs}_p - \text{obs}_m)^2,$$

where obs_p is the observed activity for structure p, pred_p is the predicted activity for structure p and obs_m is the mean observed activity for the omitted structures in the sample (20% of the train set in our case).

To evaluate the external predictive power of the model, the dataset was divided randomly into two parts by using the rule of the equal distribution of the biological activity data in both train and test sets. The R_{ext}^2 was calculated.

R-square maps were generated separately for the steric and electrostatic fields using the WLS (weighted least squares) method. The portions of the normal coordinate space, where the variation in mapped data values relates to activity, were visualized. In fact map generation is a process of discarding those points that do not correlate with the activity, and storing the R^2 values of the correlation for each remaining point.

3.1.1. Results for steric fields

In the case of steric interaction energies, the initial dataset consisting of 100 compounds was randomly separated into two groups – 75 compounds for the train set and 25 compounds for the test set. Five principal components explain 82.75% of the data dispersion. The calculated statistical parameters for the steric interaction field are as follows:

$$\begin{aligned} \text{Train series: } N &= 75; R^2 = 0.877; R_{\text{pred}}^2 = 0.752; \\ Q^2 &= 0.624; F = 98.47; s = 0.354. \\ \text{Test series: } N &= 25; R_{\text{ext}}^2 = 0.700. \end{aligned}$$

The result indicates that the model is acceptable from statistical point of view. The correlations between the predicted and observed values of $\log(1/\text{IC}_{50})$ are presented in Fig. 4 for the steric interactions in the train and test sets of molecules.

The plane projected three-dimensional WLS map in terms of steric interaction energy is presented in Fig. 5. Important parts for the steric interactions around the set of superimposed molecules can be seen from the map. The grey contours on the map show the regions, where bulky substituents favor biological activities. In contrast, the black areas correspond to steric hindrance and hence small substituents are preferred. On the basis of 3D QSAR analysis for steric interactions it can be concluded that: bulky substituents in positions 3', 4', 4'', 5'', 6 would increase biological activity. More concrete, substituents above the plane in position 3' and substituents below the plane in position 4' would have favorable influence.

3.1.2. Results for electrostatic fields

Analogous approach was used for evaluating the influence of electrostatic interactions on biological activity. In this case six principal components that explain 86.43% of the total variance statistical criteria for the electrostatic interactions are the following:

$$\begin{aligned} \text{Train series: } N &= 75; R^2 = 0.941; R_{\text{pred}}^2 = 0.813; \\ Q^2 &= 0.643; F = 180.41; s = 0.253. \\ \text{Test series: } N &= 25; R_{\text{ext}}^2 = 0.764. \end{aligned}$$

R^2 and R_{pred}^2 values are higher than those for the model of steric interactions. The obtained R_{ext}^2 value for the test series is also a proof for the model validity and quality. The correlations between the predicted and observed values of $\log(1/\text{IC}_{50})$ are presented in Fig. 6 for the electrostatic interactions in the train and test sets of molecules. The better statistical parameters include that the electrostatic interactions have more significant role in defining the observed anticancer effect of 7- and 3-substituted 1,4-dihydro-4-oxo-1-(2-thiazoly)-1,8-naphthyridines. This conclusion is in accord with the findings that SNS-595 has phosphorylative properties [37,40,41,43]. The plain projection of the three-dimensional map obtained from the 3D QSAR analysis of potential electrostatic interactions is presented in Fig. 7. Black contours represent areas where high electron density correlates with biological activity of

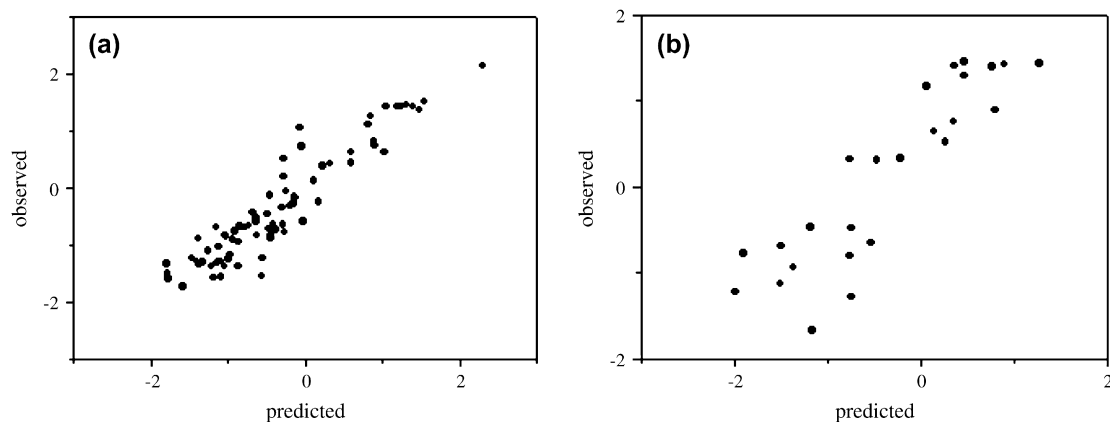


Fig. 4. Predicted versus observed activities for (a) the train set and (b) test set of the steric fields.

the aligned molecules. In contrast, the grey regions correspond to low electron density or positively charged substituents. After careful analysis of the obtained WLS map for the electrostatic interactions the important regions for the anticancer activity can be defined. Substituents conditioning relatively low electron density in positions 3', 4' and 6 have favorable influence on the biological effect. Electronegative substituents in the hydrocarbon residue in positions 2', 5', 3'' and 4'' would increase the antitumor activity of the studied series of 1,8-naphthyridine derivatives.

It can be clearly seen from the WLS maps (Figs. 5 and 7) that position 3 does not contribute to the explanation of the biological data. This conclusion is also supported by the SAR analysis of Tsuzuki et al. [3] who synthesized some additional structures with different substituents in the third position and found out that these molecules have similar biological effect.

3.2. 2D QSAR results

The 2D QSAR analysis was performed using the Fujita–Ban model [42]. Symmetric equations of Free–Wilson's De

Novo model are totally neglected in the Fujita–Ban analysis [42]. The mathematical model of the Fujita–Ban analysis can be represented by the following equation:

$$\log \text{BA} = \sum a_i x_i + \mu \quad (2)$$

where x_i is the group contribution of the substituent i , a_i is respective coefficient for the group contribution x_i . $a_i = 1$, if the substituent exists, and $a_i = 0$ if does not (i.e. for H atom). Eq. (2) was used in this work. BA is the biological activity ($1/\text{IC}_{50}$) and μ is equal to $\log(1/\text{IC}_{50})$ calculated for the unsubstituted compound, i.e. the parent compound (26), Fig. 2.

Successful application of the method required a series with constant base structure, substituted at different positions. In the present study we carried out 2D QSAR analysis employing the ring basic structure of the most active compound SNS-595 (compound 74). It is shown in Fig. 8. Forty-nine compounds fall into this group (11–18, 26–40, 45, 46, 55–71, 73–79).

The method of multi-linear regression was applied for evaluating statistical dependence. A stepwise regression was used to eliminate statistically insignificant variables. The following equation was obtained:

$$\begin{aligned} \log(1/\text{IC}_{50}) = & 0.373(\text{R}_9 - \text{H}) - 2.06(\text{R}_9 - \text{OH}) \\ & - 1.753(\text{R}_9 - \text{NO}_2) - 1.576(\text{R}_7 - \text{OH}) \\ & - 1.431(\text{R}_9 - \text{NH}_2) - 1.307(\text{R}_1 - i\text{Pr}) \\ & - 0.735(\text{R}_2 - \text{CH}_3) - 0.934(\text{R}_2 - \text{OCH}_3) \\ & + 0.355(\text{R}_7 - \text{CH}_3) + 0.307(\text{R}_7 - \text{OCH}_3) \\ & - 0.761(\text{R}_9 - \text{Cl}) + 0.501(\text{HC} - 1) \\ & - 0.733(\text{R}_{10} - \text{CF}_3) - 0.692(\text{R}_3 - \text{CH}_3) \\ & - 0.623(\text{R}_8 - \text{CH}_3) - 0.413(\text{R}_4 - \text{CH}_2\text{NH}_2) \\ & - 0.468(\text{R}_{10} - \text{Cl}) + 0.35(\text{HC} - 2) + 0.497 \end{aligned} \quad (3)$$

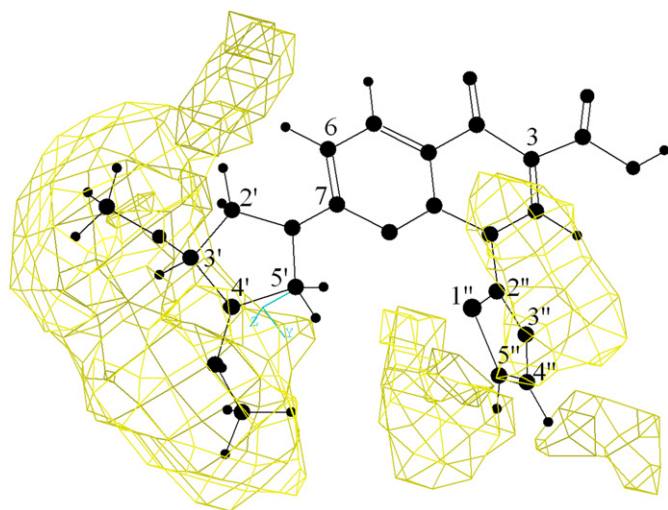


Fig. 5. WLS R^2 map for the steric interactions visualized on the structure of molecule 74.

$$N = 49; R^2 = 0.93; s = 0.214; F = 23.51.$$

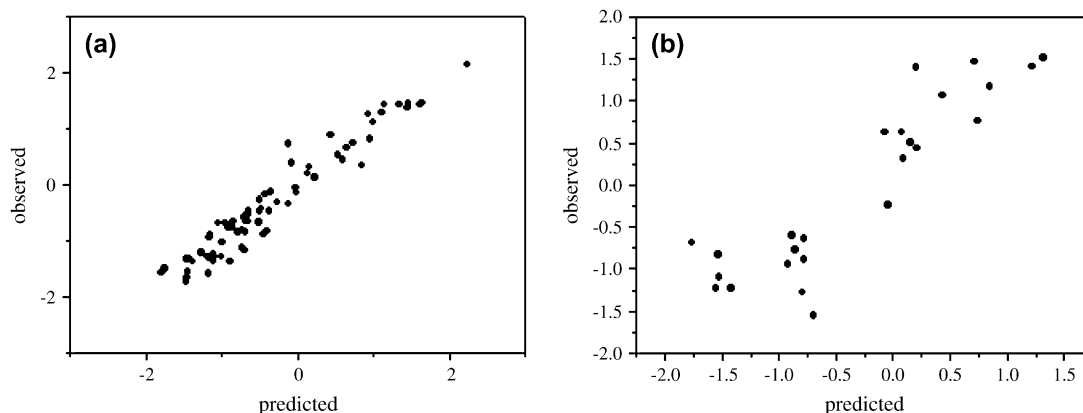


Fig. 6. Predicted versus observed activities for (a) the train set and (b) test set of the electrostatic fields.

The positive coefficients in Eq. (3) correspond to higher antitumor activity. Therefore, the lack of any group in position 6 ($R_9 = H$) would have positive influence on the biological effect. It is also favorable if the substituent R_7 in position 3' above the plane of the ring is methyl or methoxy group. The existence of two chiral centers in the molecule (labeled as HC-1 and HC-2 in Eq. (3)) is also of particular importance.

The following comparisons and considerations can be made considering the results obtained from 2D correlation analysis (Eq. (3)) and 3D maps for steric (Fig. 5) and electrostatic (Fig. 7) fields.

3.2.1. Positions 3' and 4'

The presence of substituents in these positions of the pyrrolidinyl ring of the parent structure leads to increase in the

biological effect. The 2D QSAR analysis confirms that because of the positive coefficient for the substituent R_7 in Eq. (3), the steric map (Fig. 5) shows that the presence of bulky substituents above (at position 3') and below the plane (at position 4') of the pyrrolidinyl ring would increase the anticancer activity. The electrostatic map (Fig. 7) shows that substituents with low electron density at these positions would have positive effect. We can summarize that relatively bulky substituents with low electron density (for instance alkyl groups) at positions 3' and 4' above and below the plane of the pyrrolidinyl ring, respectively, are recommended. It is important to notice that the presence of two chiral centers in the parent structure influences positively the biological activity. The important chiral centers are most probably at positions 3' and 4'. This statement is also confirmed by experimental studies [1,2].

3.2.2. Positions 2' and 5'

The 2D QSAR equation shows that the presence of CH_3 group in positions 2' and 5' (R_8 and R_3 , respectively) leads to lower activity. The electrostatic 3D map shows that the

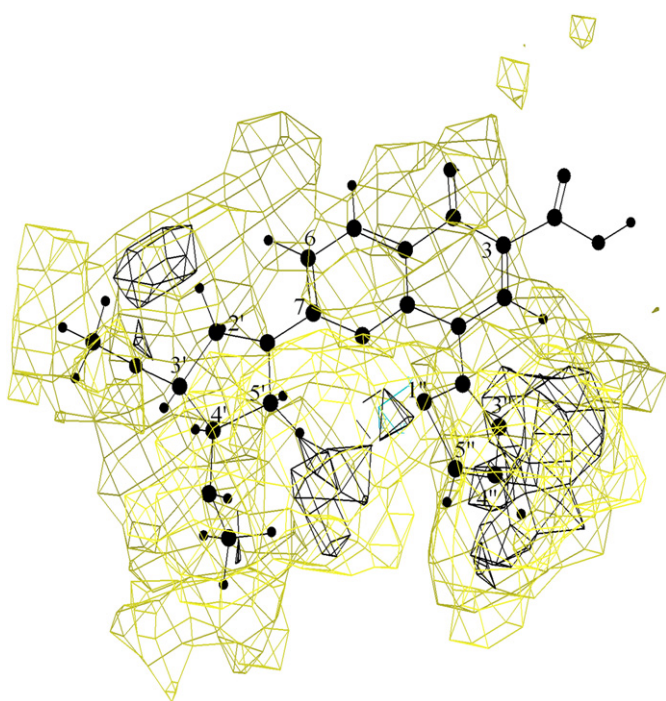


Fig. 7. WLS R^2 map for the electrostatic interactions visualized over the structure of molecule 74.

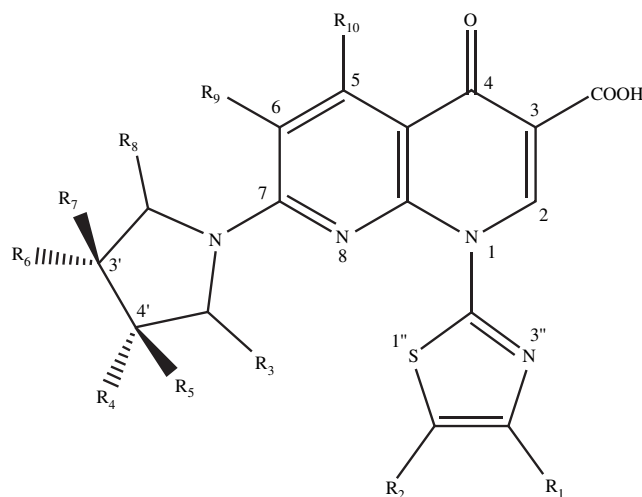
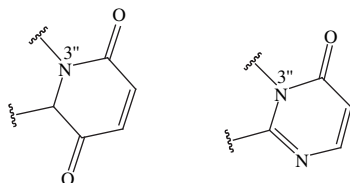
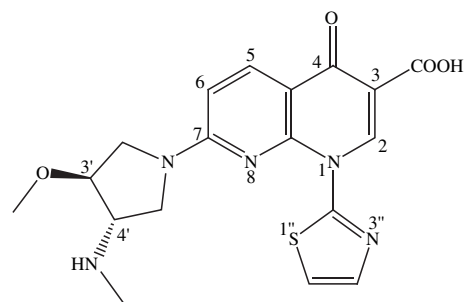


Fig. 8. Numbering of atoms for the base structure in Fujita–Ban analysis 1-(4,5-disubstituted thiazol-2-yl)-7-(2,3,3,4,4,5-hexasubstituted pyrrolidin-1-yl)-5,6-disubstituted-4-oxo-1,4-dihydro-1,8-naphthyridine-3-carboxylic acid.

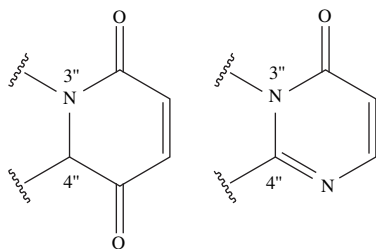
Position:6 - H, CH₃;2' - OCH₃, COCH₃;3' (over the plane) - CH₂CH₃, i-Pr;4' (under the plane) - CH(CH₃)CH₂CH₃;5' - COCH₂CH₂CH₃, COCH₂CH₃;3'' - COCH₂CH₃, COCH=CH₂; or4'' - COCH₃, OCH₃, NH₂, NHCH₃;5'' - CH(CH₂CH₃)₂, CH₂CH(CH₂CH₃)₂

Scheme 1.

presence of substituents containing electronegative atom (for example COCH₃ or OCH₃) at these positions would influence favorably the anticancer effect.

3.2.3. Positions 3'' and 4''

The regression coefficient for position 4'' (R₁) in Eq. (3) shows that bulky substituents (isopropyl in our case) lead to decreased biological effect. The steric map from 3D QSAR analysis confirms the preference of small groups at these positions (Fig. 5). Having in mind the existence of clearly expressed black areas around positions 3'' and 4'' in thiazolyl ring in the 3D electrostatic map (Fig. 7), it can be concluded that small groups, containing an electronegative atom, will have positive effect. After a detailed analysis of the black area shape around the thiazolyl ring, it is fascinating to propose the following cyclic substituents for positions 3'' and 4'':

**3.2.4. Position 6**

The regression coefficients in 2D QSAR equation (Eq. (3)) show that hydrogen atom in position 6 (R₉) is the most favorable and the presence of an electronegative atom leads to a decreased activity. The 3D electrostatic map confirms that. Having in mind the 3D QSAR analysis for electrostatic fields and the resulting map (Fig. 7), it can be summarized that small substituents with low electron density at position 6 would increase the anticancer effect.

The results obtained allow proposing a number of possible substitutions into the backbone structure that are expected to enhance the antitumor activity of compounds from the 1,8-naphthyridine series. Possible substitutions leading to enhanced activities, proposed on the basis of the relationships found, are shown in Scheme 1.

4. Conclusions

The 2D and 3D QSAR analyses allow to derive the following principal conclusions regarding the relationships between chemical and electronic structure and anticancer activity for the series of 7- and 3-substituted 1,4-dihydro-4-oxo-1-(2-thiazolyl)-1,8-naphthyridines:

- Substituents with low electron density and small size at the sixth position have positive effect on the anticancer activity against Murine P388 Leukemia cells.
- The presence of substituents containing an electronegative atom at positions 2' and 5' increases the antitumor effect.
- Bulky substituents with low electron density at positions 3' (above the pyrrolydine ring plane) and at position 4' (below the plane) enhance the antitumor activity.
- The presence of substituents with small size and having an electronegative atom in the hydrocarbon residue at positions 3'' and 4'' increases the anticancer activity.

References

- [1] K. Tomita, Y. Tsuzuki, K. Shibamori, M. Tashima, F. Kajikawa, Y. Sato, S. Kashimoto, K. Chiba, K. Hino, J. Med. Chem. 45 (2002) 5564–5575.
- [2] Y. Tsuzuki, K. Tomita, K. Shibamori, Y. Sato, S. Kashimoto, K. Chiba, J. Med. Chem. 47 (2004) 2097–2109.
- [3] Y. Tsuzuki, K. Tomita, Y. Sato, K. Shibamori, S. Kashimoto, K. Chiba, Bioorg. Med. Chem. Lett. 14 (2004) 3189–3193.

- [4] D.T.W. Chu, P.B. Fernandes, in: B. Testa (Ed.), *Advances in Drug Research*, vol. 21, Academic Press, New York, 1991, pp. 39–144.
- [5] D.C. Hooper, *Drugs* 58 (Suppl. 2) (1999) 6–10.
- [6] J.M. Berger, S.J. Gamblin, S.C. Harrison, J.C. Wang, *Nature* 379 (1996) 225–232.
- [7] H. Malonne, G. Atassi, *Anticancer Drugs* 8 (1997) 811–822.
- [8] D.A. Burden, N. Osheroff, *Biochim. Biophys. Acta* 1400 (1998) 139–154.
- [9] Y. Yamashita, T. Ashizawa, M. Morimoto, J. Hosomi, H. Nakano, *Cancer Res.* 52 (1992) 2818–2822.
- [10] M.J. Suto, J.M. Domagala, G.E. Roland, G.B. Maillour, M.A. Cohen, *J. Med. Chem.* 35 (1992) 4745–4750.
- [11] K. Hoshino, K. Sato, K. Akahane, A. Yoshida, I. Hayakawa, M. Sato, T. Une, Y. Osada, *Antimicrob. Agents Chemother.* 35 (1991) 309–312.
- [12] K. Hoshino, K. Sato, T. Une, Y. Osada, *Antimicrob. Agents Chemother.* 33 (1989) 1816–1818.
- [13] D.T.W. Chu, *Drugs Future* 17 (1992) 1101–1109.
- [14] S.J. Froelich-Ammon, P.R. McGuirk, T.D. Gootz, M.R. Jefson, N. Osheroff, *Antimicrob. Agents Chemother.* 37 (1993) 646–651.
- [15] G.H. Kuo, M.A. Eissenstat, M.P. Wentland, R.G. Robinson, K.M. Klingbeil, D.W. Danz, S.A. Coughlin, *Bioorg. Med. Chem. Lett.* 5 (1995) 399–404.
- [16] M.P. Wentland, S.C. Aldous, M.D. Gruett, R.B. Perni, R.G. Powles, D.W. Danz, K.M. Klingbeil, A.D. Peverly, R.G. Robinson, T.H. Corbett, J.B. Rake, S.A. Coughlin, *Bioorg. Med. Chem. Lett.* 5 (1995) 405–410.
- [17] M.A. Eissenstat, G.H. Kuo, J.D. Weaver, M.P. Wentland, R.G. Robinson, K.M. Klingbeil, D.W. Danz, T.H. Corbett, S.A. Coughlin, *Bioorg. Med. Chem. Lett.* 5 (1995) 1021–1026.
- [18] J.F. Barrett, T.D. Gootz, P.R. McGuirk, C.A. Farrell, S.A. Sokolowski, *Antimicrob. Agents Chemother.* 33 (1989) 1697–1703.
- [19] M.J. Robinson, B.A. Martin, T.D. Gootz, P.R. McGuirk, M. Moynihan, J.A. Sutcliffe, N. Osheroff, *J. Biol. Chem.* 266 (1991) 14585–14592.
- [20] M.J. Robinson, B.A. Martin, T.D. Gootz, P.R. McGuirk, N. Osheroff, *Antimicrob. Agents Chemother.* 36 (1992) 751–756.
- [21] S.H. Elsea, N. Osheroff, J.L. Nitissll, *J. Biol. Chem.* 267 (1992) 13150–13153.
- [22] M.P. Wentland, G.Y. Leshner, M. Reuman, M.D. Gruett, B. Singh, S.C. Aldous, P.H. Dorff, J.B. Rake, S.A. Coughlin, *J. Med. Chem.* 36 (1993) 2801–2809.
- [23] P.A. Permana, R.M. Snapka, L.L. Shen, D.T.W. Chu, J.J. Clement, J.J. Plattner, *Biochemistry* 33 (1994) 11333–11339.
- [24] D.T. Chu, R. Hallas, J.J. Clement, J. Alder, E. McDonald, J.J. Plattner, *Drugs Exp. Clin. Res.* 18 (1992) 275–282.
- [25] S.C. Kuo, H.Z. Lee, J.P. Juang, Y.T. Lin, T.S. Wu, J.J. Chang, D. Lednicer, K.D. Paull, C.M. Lin, E. Hamel, K.H. Lee, *J. Med. Chem.* 36 (1993) 1146–1156.
- [26] L. Li, H.K. Wang, S.C. Kuo, T.S. Wu, D. Lednicer, C.M. Lin, E. Hamel, K.H. Lee, *J. Med. Chem.* 37 (1994) 1126–1135.
- [27] L. Li, H.K. Wang, S.C. Kuo, T.S. Wu, A. Mauger, C.M. Lin, E. Hamel, K.H. Lee, *J. Med. Chem.* 37 (1994) 3400–3407.
- [28] K. Chen, S.C. Kuo, A. Mauger, C.M. Lin, E. Hamel, K.H. Lee, *J. Med. Chem.* 40 (1997) 2266–2275.
- [29] Z. Ji, K.H. Wang, K.F. Bastow, X.K. Zhu, S.J. Cho, Y.C. Cheng, K.L. Lee, *Bioorg. Med. Chem. Lett.* 7 (1997) 607–612.
- [30] K. Chen, S.C. Kuo, M.C. Hsieh, A. Mauger, C.M. Lin, E. Hamel, K.H. Lee, *J. Med. Chem.* 40 (1997) 3049–3056.
- [31] Y. Xia, Z.Y. Yang, P. Xia, K.F. Bastow, Y. Tachibana, S.C. Kuo, E. Hamel, T. Hackl, K.H. Lee, *J. Med. Chem.* 41 (1998) 1155–1162.
- [32] S.X. Zhang, K.F. Bastow, Y. Tachibana, S.C. Kuo, E. Hamel, A. Mauger, V.L. Narayanan, K.H. Lee, *J. Med. Chem.* 42 (1999) 4081–4087.
- [33] M.J. Hour, L.J. Huang, S.C. Kuo, Y. Xia, K. Bastow, Y. Nakanishi, E. Hamel, K.H. Lee, *J. Med. Chem.* 43 (2000) 4479–4487.
- [34] Y. Xia, Z.Y. Yang, M.J. Hour, S.C. Kuo, P. Xia, K.F. Bastow, Y. Nakanishi, P. Nampoothiri, T. Hackl, E. Hamel, K.H. Lee, *Bioorg. Med. Chem. Lett.* 11 (2001) 1193–1196.
- [35] Y.Y. Lai, L.J. Huang, K.H. Lee, Z. Xiao, K.F. Bastow, T. Yamoric, S.C. Kuo, *Bioorg. Med. Chem.* 13 (2005) 265–275.
- [36] H.I. El-Subbagh, A.H. Abadi, I.E. Al-Khawad, K.A. Al-Rashood, *Arch. Pharm. Pharm. Med. Chem.* 101 (1999) 19–24.
- [37] U. Hoch, J. Hyde, M.A. Nannini, M.J. Evanchik, C.E. Lawrence, M.R. Arkin, D.H. Walker, J.A. Silverman, 96th Annual American Association for Cancer Research Meeting (2005) Anaheim, CA, Abstract No 2277, http://sunesis.com/pdf/Sunesis_PDPPoster_final.pdf.
- [38] J. Wright, J. Hyde, J.A. Silverman, D.H. Walker, M.R. Arkin, 97th Annual American Association for Cancer Research Meeting (2006), Washington D.C., Abstract No 2132, http://sunesis.com/pdf/poster1_04_06.pdf.
- [39] R. Advani, M. Gordon, H. Hurwitz, D. Mendelson, H. Wakelee, S. Ebbinghaus, U. Hoch, J.A. Silverman, N. Havrilla, D. Adelman, *J. Clin. Oncol.* 23 (2005) 159S.
- [40] J. Hyde, J. Wright, J.A. Silverman, D.H. Walker, M.R. Arkin, 96th Annual American Association for Cancer Research Meeting (2005) Anaheim, CA, Abstract No 2285, http://sunesis.com/pdf/Sunesis_apoptosisfinal.pdf.
- [41] U. Hoch, M.J. Evanchik, J.A. Silverman, *Clin. Cancer Res.* 11 (2005) 9154S.
- [42] J. Hyde, J. Wright, N. Osheroff, J.A. Silverman, D.H. Walker, M.R. Arkin, 96th Annual American Association for Cancer Research Meeting (2005) Anaheim, CA, Abstract No 2293, http://sunesis.com/pdf/Sunesis_cellcyclefinal1.pdf.
- [43] J. Hyde, J. Wright, D.H. Walker, J.A. Silverman, M.R. Arkin, 97th Annual American Association for Cancer Research Meeting (2006) Washington D.C., Abstract No 2074, http://sunesis.com/pdf/poster2_04_06.pdf.
- [44] Chem-X, Chem-X was developed at Chemical Design Ltd. (now part of Accelrys), 2000.
- [45] T. Fujita, T. Ban, *J. Med. Chem.* 14 (1971) 148–152.
- [46] S.M. Free Jr., J.W. Wilson, *J. Med. Chem.* 7 (1964) 395–399.
- [47] I.C. Muszynski, L. Scapozza, K.-A. Kovar, G. Folkers, *Quant. Struct. Act. Relat.* 18 (1999) 342–353.
- [48] Z. Weifan, E.G. Srinivas, C.S. Jin, A. Tropsha, 215th ACS National Meeting, Comparative studies of 3D (CoMFA) and 2D QSAR methods, Book of Abstracts, Am. Chem. Soc., Washington, 1998.
- [49] U.C. Singh, P.K. Weiner, J. Caldwell, P.A. Kollman, AMBER Version 3, developed at the University of California at San Francisco, 1986.
- [50] H. Kubinyi, *Pharm. Acta Helv.* 69 (1995) 259–269.